Neuron Segmentation with Level Sets

Suvadip Mukherjee[1], Barry Condron[2] and Scott T. Acton[1]
{sm5vp, bc4f, sa4e}@virginia.edu
[1]C.L. Brown Department of Electrical and Computer Engineering & [2]Department of Biology
University of Virginia
Charlottesville, VA 22904

***Abstract*— We propose a variational scheme for neuron segmentation. The growing demand for an automated image analysis tool for efficient segmentation of neurites has led to significant focus and advancement in the field of neuro-image analysis. However, the complex structure of the neurites and imaging artifacts pose considerable challenge for automated image analysis. Analysis of the neuronal morphology is important to determine the cause of certain neurological diseases (e.g. Alzheimer's disease). Such applications demand accurate segmentation of the neuron that respect the geometric structure as well as the branching patterns. Our proposed method relies on level set evolution to perform segmentation. The propagation of the level sets is primarily governed by a medial flow vector field, which encourages the growth of the level set along the width and the axis of the vascular neurite structures. Experimental results on both 2D and 3D images suggest that the method is robust to imaging artifacts and is efficient in capturing the complex branching structures of the neurons.**

***Inext Terms*—** Vessel segmentation, active contours, biological imaging

I. INTRODUCTION

Automated analysis of the morphological structure of neurons has been a major challenge for image analysts. The importance of the problem is highlighted by the fact that recent advances in the field of microscopy have enabled the biologists to acquire a significant amount of data. In fact, a major bottleneck in developing the neuronal map (or Neurome) of an organism is the lack of proper tools for automated image analysis. Although this problem of neuron segmentation has received considerable attention in the last few years, manual or semi-manual segmentation tools is still considered the gold standard for the job. With almost 20,000 neurons in the VNC of the fruit fly Drosophila, the success of the Neurome project largely depends on high quality automated segmentation methods.

In this paper, we primarily focus on the problem of segmenting neurons from 2D/3D images. The confocal microscopy images are obtained from the Biology department at UVa. Also, to demonstrate the wide applicability of our method, we show our results on 2D retinal blood vessel images from the publicly available DRIVE database.

Figure 1 shows two neuron images of the Drosophila by confocal microscopy.

This work was supported in part by the NSF (1062433).

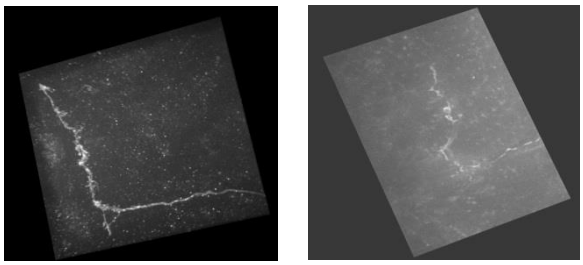

Figure 1: 2D projection of the 3D confocal microscopy image of Drosophila larvae neuron

These images are obtained by staining the Drosophila larvae with standard fluorescence proteins (e.g. GFP) and then imaging the fluorescing cells. Similar to any light microscopy imaging techniques, the picture quality is hampered due to the presence of background clutter (non-neuronal structures) and contrast inhomogeneity. An efficient segmentation tool should be able to handle the non-neuronal structures (or structured noise) and also deal with the changes in foreground contrast.

The state of the art tracing tools can be broadly categorized in two categories: The first set of methods relies on manually or semi-manually chosen seed points to initiate the tracing ([1]-[4]). These algorithms are computationally simpler, since the computation is performed on a set of pre-selected points and its neighborhood. However, while manual selection of seed points is time consuming and prone to human error, automatic selection of seeds is still an open problem. Since the foundation of these techniques lie in proper seed selection, the seed-based methods suffer heavily in absence of robust initialization methods. Moreover, additional care needs to be taken to preserve the branching patterns of the neurons. A second set of tools have been developed, which relies on traditional image segmentation routines, followed by reconstruction of the neuronal structures using Minimum Spanning Tree ([5]). These methods rely on good quality segmentation and noise free skeletonization of the object to detect the neurite centerlines. The quality of the segmentation routine heavily impacts the final output, and although these methods are typically robust to detecting branches, one needs to post process the final result to eliminate the non-neuronal structures. A nice review of the latest neuron tracing methods is presented in [6].

II. LEVEL SETS FOR NEURON SEGMENTATION

Based on our dataset, we hypothesize that an efficient neuron tracer should be able to (a) detect and remove background clutter, (b) distinguish between neuronal and non-neuronal structures and (c) respect the geometric shape and branching pattern of the neurons. Variational segmentation techniques using level sets ([7]-[9]) have gained popularity due to their natural adaptability to topology changes in the object. In fact, the region based curve evolution approaches [8] are efficient in dealing with images where edge based methods are prone to error. In this paper, we formulate a novel level set evolution framework to segment the neuronal segments. Since level set based methods are robust to topological changes, we do not require additional post processing routines to preserve the important morphological structures like junctions and branches. Also, our method can deal with background clutter, which may be removed by analyzing the Hessian matrix of the image. The topology adaptive property of level set methods encourages the preservation of non-neuronal elongated structures. This problem can be eradicated by using morphological filters to control the topology of the evolving level sets. In the following subsections we introduce our formulation and the mathematical framework for segmentation.

A. Medial Flow Vector Field

Frangi et al. [10] proposed a method to distinguish between tubular and non-tubular structures in digital images. Using the prior information that the neurites are tubular in shape, the eigenvalues of the Hessian matrix is analyzed to emphasize the tubes. This operation is performed in scale space to allow preserve structures with multiple widths. Formally, the scale space *vesselness* score $\mathcal{N}_\sigma$ is computed at each pixel (voxel) $\mathbb{p}$ (at scale σ) as follows

$$\mathcal{N}_\sigma(\mathbb{p}) = \begin{cases} \dfrac{|\lambda_1(\mathbb{p}) - \lambda_2(\mathbb{p})|^2}{(|\lambda_1(\mathbb{p})||\lambda_2(\mathbb{p}) - \lambda_3(\mathbb{p})|)} & \text{if } \lambda_2(\mathbb{p}), \lambda_3(\mathbb{p}) \le 0 \\ 0 & \text{otherwise} \end{cases} \quad (1)$$

$\lambda_1, \lambda_2, \lambda_3$ are the eigenvalues of the hessian of the image, corresponding to the eigenvectors $\boldsymbol{v_1}, \boldsymbol{v_2}, \boldsymbol{v_3}$. The computed vesselness score at the correct scale enhances the tubular structure, while eliminating blobs, discs and noise. It is observed that the eigenvector $\boldsymbol{v_1}$ is oriented in the direction of minimum curvature, i.e. in the direction of the vessel. The two other orthonormal eigenvectors point outwards, signifying maximum curvature (Fig.2).

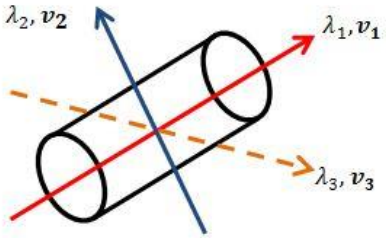

Figure 2: Ideal eigenvector directions for a tubular structure

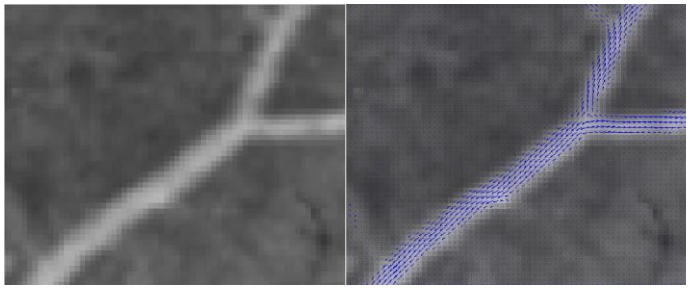

(a) (b)

Figure 3: (a) 2D neuron segment and (b) the medial flow vector field shown by blue arrows.

With this background, let us now introduce the medial flow vector field. If $f(\mathbb{p})$ be the grayscale digital image with domain $\Omega = \mathbb{R}^3$ ($\mathbb{p} \in \mathbb{R}^3$), we define the medial flow vector field as

$$\boldsymbol{F_1}(\mathbb{p}) = \begin{cases} \mathcal{M}_1(\mathbb{p})\boldsymbol{v_1}(\mathbb{p}) & \text{if } \lambda_2(\mathbb{p}), \lambda_3(\mathbb{p}) \le 0 \\ 0 & \text{otherwise} \end{cases} \quad (2)$$

$\mathcal{M}_1(\mathrm{x})$ is the magnitude of the vector field at the location x. As illustrated in Fig.3, this vector field indicates the axial direction of the cylindrical neurites. The magnitude function is chosen such that the vector field is more prominent in the neuronal portions. Apart from the medial flow field, we can also define two orthonormal vector fields, $\boldsymbol{F_1}(\mathbb{p})$ and $\boldsymbol{F_2}(\mathbb{p})$ as

$$\boldsymbol{F_j}(\mathbb{p}) = \begin{cases} \mathcal{M}_j(\mathbb{p})\boldsymbol{v_j}(\mathbb{p}) & \text{if } \lambda_2(\mathbb{p}), \lambda_3(\mathbb{p}) \le 0 \\ 0 & \text{otherwise} \end{cases} \quad \mathrm{j}=2,3$$

These vector fields are orthogonal to the medial flow field and are oriented towards the vessel edges. $\mathcal{M}_2$, $\mathcal{M}_3$ are the magnitudes of the vector fields.

Choosing a suitable magnitude function is an important engineering issue. Intuitively, the magnitude function should be chosen such that the vector fields are dominant in presence of tubular structures. Since the neurons are brighter than the background, we define the magnitude function as follows

$$\mathcal{M}_j(\mathbb{p}) = kf(\mathbb{p}) + (1-k)\mathcal{N}(\mathbb{p}),\ j = \{1,2 \text{ or } 3\}.$$

$\mathcal{N}(\mathbb{p}) = \max_{\sigma_{min}<\sigma<\sigma_{max}} \mathcal{N}_\sigma(\mathbb{p})$ is the scale space vesselness score over the range of scales. The convex combination, parameterized by the constant $\mathrm{k} \in (0,1)$ emphasizes the junctions and end points, which are often less enhanced by the Frangi filter. In all our experiment, we fix $\mathrm{k} = 0.1$.

B. Mathematical Framework for Level Set Evolution

The level set evolution is guided by the vector fields defined in the previous subsection. Our objective is to evolve a level set function from a preselected seed along the medial flow field. The evolution equation is obtained by minimizing the following energy functional

(a) initial (b) 10 iterations (c) 20 iterations (d) convergence

Figure 4: Level set evolution at different time steps to segment the tubular structure in Figure 3

$$E(\Phi) = E_1(\Phi) + \nu \int_{\Omega} \left(1 - \left|\left|\nabla \Phi\right|\right|\right)^2 dx \qquad (3)$$

Φ is the signed distance function for level set evolution which is strictly positive at points inside the object and negative for the points outside. The object boundary can be obtained by computing the zero level set of Φ. The vector $\nabla\Phi(\mathrm{x})$ represents the gradient of the level set function at $\mathrm{x} \in \Omega$.

The segmentation is performed by minimizing the functional $E(\Phi)$ with respect to Φ. Let us discuss the contribution of the different terms in (3). The second term contributes to the smoothing of the level set function (LSF). Since for a signed distance function Φ, $||\nabla\Phi|| = 1$, minimizing this term facilitates the level set function to be faithful to the signed distance function property. Also, this eliminates the need for periodic manual re-initialization of the LSF [9]. ν is a parameter, which controls the influence of the regularizer term to the energy functional. Selection of ν depends on the signal to noise ratio of the image. A discussion on the selection of ν is presented in [9].

Evolution of level set function is governed by the first term ($E_1(\Phi)$). This can be written as

$E_1(\Phi) = E_{11}(\Phi) + E_{12}(\Phi) + E_{13}(\Phi)$ where

$$E_{11}(\Phi) = -\int_{\mathrm{x}\in\Omega} < \boldsymbol{F_1}(\mathrm{x}), \frac{\nabla\Phi(\mathrm{x})}{||\nabla\Phi(\mathrm{x})||} >^2 \mathrm{H}(\Phi) d\mathrm{x}\,,$$

$$E_{12}(\Phi) = -\int_{\mathrm{x}\in\Omega} < \boldsymbol{F_2}(\mathrm{x}), \frac{\nabla\Phi(\mathrm{x})}{||\nabla\Phi(\mathrm{x})||} >^2 \mathrm{H}(\Phi) d\mathrm{x} \quad \text{and}$$

$$E_{13}(\Phi) = -\int_{\mathrm{x}\in\Omega} < \boldsymbol{F_3}(\mathrm{x}), \frac{\nabla\Phi(\mathrm{x})}{||\nabla\Phi(\mathrm{x})||} >^2 \mathrm{H}(\Phi) d\mathrm{x}.$$

$< \boldsymbol{m}, \boldsymbol{n} >$ denotes the inner product of the vectors $\boldsymbol{m}$ and $\boldsymbol{n}$. $\mathrm{H}(\Phi)$ is the unit step function or the Heaviside function. Minimizing $E_{11}(\Phi)$ has the effect of stretching the object area to cover the width of a vessel. Propagation of the zero level set of Φ along the vessel axis is obtained by minimizing $E_{12}(\Phi)$ and $E_{13}(\Phi)$. The minimizing LSF tries to align the level set normal vectors $\frac{\nabla\Phi(\mathrm{x})}{||\nabla\Phi(\mathrm{x})||}$ along the force fields by minimizing the inner product, thus stretching the object boundary to cover the axial length and the width of the vessel. This is illustrated in Figure 4.

The functional in (3) can be minimized using the calculus of variation. The optima can be numerically computed using the gradient descent method. Such numerical methods are known to converge to local minima, which my yield undesired segmentation. In fact, the final segmentation may contain disjoint components due to contrast variation i0n the neurites. Although the connectivity between the components may be analyzed using the Tree2Tree algorithm [5], we propose a simple solution to this problem. The minimization of (3) does not constrain the number of connected components in the final solution, which allows multiple disjoint components to appear. We now minimize $E(\Phi)$ with the constraint $\zeta\big(\mathrm{H}(\Phi)\big) \leq p$. ζ is a function that counts the number of connected components in a binary image. Here p is an integer that specifies the number of permissible components in the result. This can be viewed as a topology controlling constraint on the LSF.

C. Discussion

Equation (3) along with the topology controlling constraint discussed above describes our framework for segmentation. However, the constraint imposed on the functional is inherently a combinatorial quantity, which makes it difficult to unify with the continuous domain formulation in (3). We take a two-step approach to approximate the solution of this optimization problem: First, we minimize (3) using traditional gradient descent method. In this paper, we only state the result for computing minima via gradient descent:

$$\frac{\partial\Phi}{\partial t} = \sum_{i=1}^{3} \left\{ \beta_i^2 \delta(\Phi) - 2\left\{ \mathrm{div}\left(\frac{\beta_i}{||\nabla\Phi||}\boldsymbol{F_i}\right) - \mathrm{div}\left(\left(\frac{\beta_i}{||\nabla\Phi||}\right)^2 \nabla\Phi\right)\right\}\mathrm{H}(\Phi)\right\} - \nu\left\{\nabla^2\Phi - \mathrm{div}\left(\frac{\nabla\Phi}{||\nabla\Phi||}\right)\right\} \qquad (4)$$

$\beta_i = < \boldsymbol{F_i}, \frac{\nabla\Phi}{||\nabla\Phi||} >$. The dummy variable t is introduced for iterative computation of the LSF. The LSF is iteratively updated according to (4).

To include the topology constraint in the evolution, we use mathematical morphology. Our objective is to obtain the neuronal structure as the largest connected component in the solution. The nearby components are merged using morphological open-close filter. After application of the open-close filter, an area based connected filter [11] is used to preserve at most p connected components. The signed distance function is re-initialized at this point to continue evolution according to (4). The two steps described above are repeated

sequentially until convergence, at which point no significant change in the LSF is observed.

III. Experimental results

The discussed method is applicable to both 2D and 3D image data. Also, our formulation is not limited to extracting neuronal structures. It is a generalized framework, which can efficiently segment vascular structures from the background. To demonstrate the efficacy of our approach, we present segmentation results on both 2D and 3D data. Segmentation results are also demonstrated for non-neuronal structures which highlights the broader applicability of the proposed method.

The 3D images are obtained from Dr. Barry Condron's laboratory at the University of Virginia. The dataset consists of ten confocal images of a GFP labeled neuron from the ventral nerve cord (VNC) of the central nervous system of the fruit fly Drosophila. These images are plagued by background clutter and have poor signal to noise ratio. The 2D image dataset consists of ten retinal blood vessel images from the publicly available DRIVE database [12]. The dataset contains retinal images which are characterized by better SNR, but complicated structure of the blood vessels.

Quantitative evaluation of the segmentation is obtained by computing the mean absolute error (MAE) between the segmentation result and the ground truth. For the neuron database, the ground truth is obtained by manually segmenting the neurons using the tracing tool Vaa3D [13]. For the 2D dataset, we make use of available manual segmentation results [12].

The discussed approach relies on the choice of a few parameters. The parameter k regulates the magnitude of the vector fields. In all our experiments, the value of k is chosen as 0.1. The image intensity term is associated with a lower weight to suppress the imaging artifacts to appear in the solution. The constant ν controls the effect of smoothing of the LSF. This value is fixed to 0.033 as suggested by the authors in [9]. Further research is required to automate the selection of a few parameters, which would make the algorithm more robust. Also, for computational purpose, the Heaviside function $H(\Phi)$ and the Dirac delta function $\delta(\Phi)$ are replaced by their smooth, regularized counterparts as described in [8].

Five 2D segmentation results and three sample 3D tracings are shown in Figure 6 and Figure 5 respectively. The segmentation result is skeletonized and a quantitative performance metric is computed by calculating the normalized MAE [5], to calculate the deviation of the obtained skeleton from the ground truth. The average MAE for the 2D dataset was 1.41%, and the average MAE was 1.12% for the 3D neuron dataset.

IV. Conclusion

We have presented a framework for automated segmentation of neurons from 3D images. The technique is able to distinguish neuronal structures from background clutter and is effective in dealing with contrast inhomogeneity. Also, the method shows promise for a variety of biological and biomedical images that involve filamentous structures. The efficacy of the algorithm is demonstrated by the results on both 2D and 3D images.

IV. References

[1] J. Lu, J. Fiala and J. L. Lichtman, "Semi-automated reconstruction of neural processes from large numbers of fluorescence images," *PLoS One*, vol. 4, 2009.

[2] H. Peng, Z. Z. Ruan, D. Atasoy and S. Sternson, "Automatic reconstruction of 3D neuron structures using a graph-augmented deformable mode," *Bioinformatics*, vol. 26, pp. 38-46, 2010.

[3] H. Peng, F. Long and G. Myers, "Automatic 3D neuron tracing using all-path pruning," *Bioinformatics*, vol. 27, pp. 239-247, 2011.

[4] Y. Wang, A. Narayanaswamy, C.-L. Tsai and B. Roysam, "A Broadly Applicable 3-D Neuron Tracing Method Based on Open-Curve Snake," *Neuroinform*, pp. 193-217, 2011.

[5] S. Basu, A. Aksel, B. Condron and S. T. Acton, "Segmentation and tracing of single neurons from 3D confocal microscope images," *IEEE Journal of Biomedical and Health Informatics*, vol. 17, pp. 319-335, 2012.

[6] E. Meijering, "Neuron Tracing in Perspective," *Cytometry Part A*, vol. 77, pp. 693-704, 2010.

[7] S. Osher and J. Sethian, "Fronts propagating with curvature-dependent speed: Algorithms based on Hamilton–Jacobi formulations," *Comput. Phys*, vol. 79, pp. 12-49, 1988.

[8] T. F. Chan and L. A. Vese, "Active Contours Without Edges," *IEEE Trans. on Image Processing*, vol. 10, pp. 266-277, 2001.

[9] C. Li, C. Xu, C. Gui and M. Fox, "Level Set Evolution Without Re-initialization: A New Variational Formulation," in *IEEE Computer Society Conference on Computer Vision and Pattern Recognition*, 2005.

[10] A. F. Frangi, W. J. Niessen, K. L. Vincken and M. A. Viergever, "Multiscale vessel enhancement filtering," in *Medical Image Computing and Computer-Assisted Intervention — MICCAI'98*, vol. 1496, Heidelberg, Springer Berlin, 1998, pp. 130-137.

[11] P. Salembier, J. Serra, "Flat zones filtering, connected operators, and filters by reconstruction," *IEEE Trans. On Image Processing*, vol 4, pp. 1153-60, 1995.

[12] J. Staal, M. Abramoff, M. Niemeijer, M. Viergever and B. v. Ginneken, "Ridge based vessel segmentation in color images of the retina," *IEEE Trans. on Medical Imaging*, vol. 23, pp. 501-509, 2004.

[13] H. Peng, Z. Ruan, F. Long, J. Simpson and E. and Myers, "V3D enables real-time 3D visualization and quantitative analysis of large-scale biological image data sets," *Nature Biotechnology*, vol. 28, pp. 348-353, 2010.

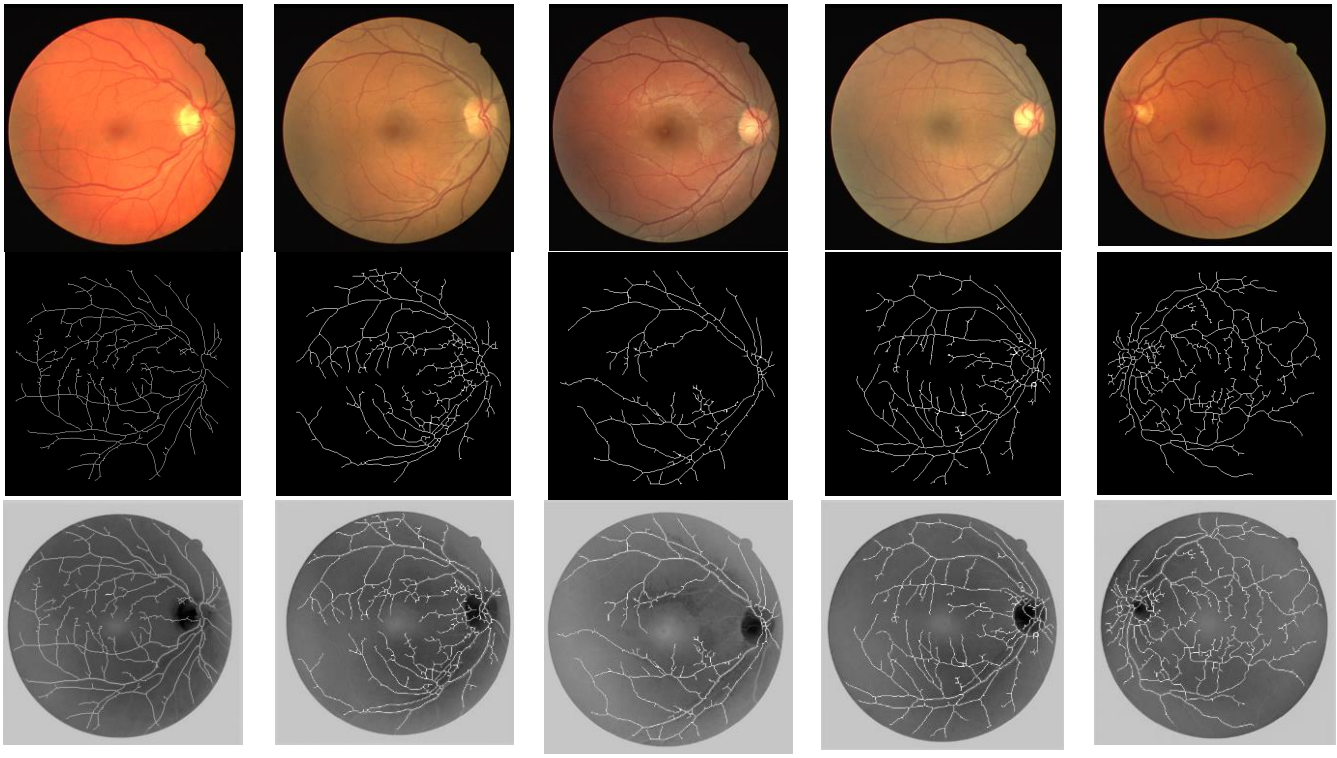

Figure 6: Segmentation results on the DRIVE dataset. The top row shows the retinal images. Skeletons of the blood vessels obtained by segmentation are shown in the second row. The segmentation results are superimposed on the image in the last row.

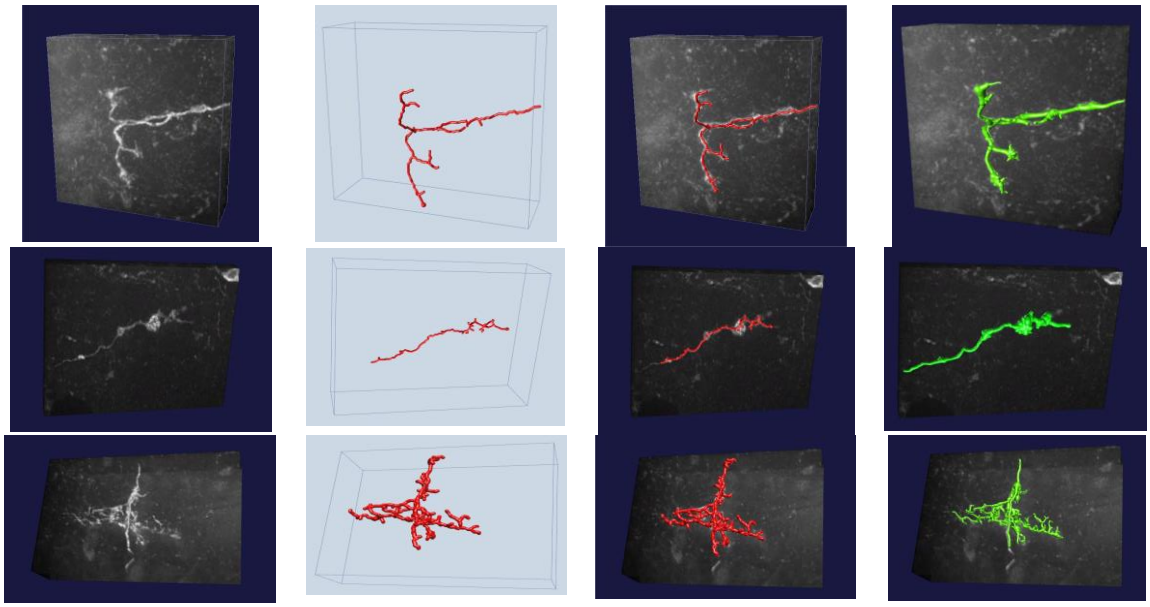

Figure 5: 3D Neuron segmentation results